RSC Advances

PAPER

View Article Online
View Journal | View Issue

Cite this: *RSC Adv.*, 2025, **15**, 16348

Fabrication of bimetallic RuCu/HAP catalysts for the selective synthesis of C_{11} biofuel precursors from biomass-based 5-methylfurfural†

Conghao Ku, ‡[b] Jiaming Tang,‡[b] Xucheng Li,[b] Zhengli Liu *[a] and Weiran Yang*[b]

The synthesis of bis(5-methylfuran)methane (BMFM) from biomass-based 5-methylfurfural (5-MF), a vital fuel precursor, is crucial for biomass refining. However, selective BMFM production from 5-MF needs to suppress side reactions such as hydrogenolysis and decarbonylation. Therefore, direct hydrogenation of 5-MF into BMFM is very challenging in sustainable biomass valorization. In this study, we developed a bimetallic RuCu/hydroxyapatite (HAP) catalyst for selective synthesis of BMFM from 5-MF. The RuCu/HAP catalyst delivered a BMFM yield of 75.6% under mild reaction conditions (V_{water} : $V_{cyclohexane}$ = 1 : 1, 4 MPa H_2, 100 °C, 4 h), significantly surpassing its monometallic counterparts (Ru/HAP: 28.7%; Cu/HAP: 0%). Furthermore, a 79% yield of C_{11} straight-chain alkanes was obtained from BMFM through the hydrodeoxygenation (HDO) process. The systematic characterization revealed that Ru mediates hydrogenation steps *via* C=O activation, while Cu orchestrates acid sites essential for self-condensation of 5-MFA. The synergistic interplay between metallic Ru and acidic Cu sites thereby enables simultaneous optimization of conversion efficiency and BMFM selectivity. These findings provide a practical and efficient route for converting lignocellulosic derivatives into renewable biofuels, particularly for sustainable aviation fuel applications.

Received 16th April 2025
Accepted 9th May 2025

DOI: 10.1039/d5ra02666k

rsc.li/rsc-advances

1 Introduction

Since the Industrial Revolution, global energy demand has persistently escalated alongside technological advancements and exponential population growth. Contemporary industrial systems remain predominantly dependent on non-renewable fossil resources (petroleum, coal and natural gas) for both fuel and chemical production. However, the non-renewable nature of these resources, coupled with their CO_2 emission-induced greenhouse effect, has necessitated the urgent development of sustainable energy alternatives.[1,2] Lignocellulose, a promising renewable biomass, has emerged as an attractive carbon resource that does not compete with food supplies for generating value-added chemicals and high-quality fuel products. Traditional aviation biofuel synthesis technologies (such as fast pyrolysis and gasification, Fischer–Tropsch synthesis) suffer from low overall process yields and high energy consumption.[3] Consequently, jet fuel production from lignocellulose-derived

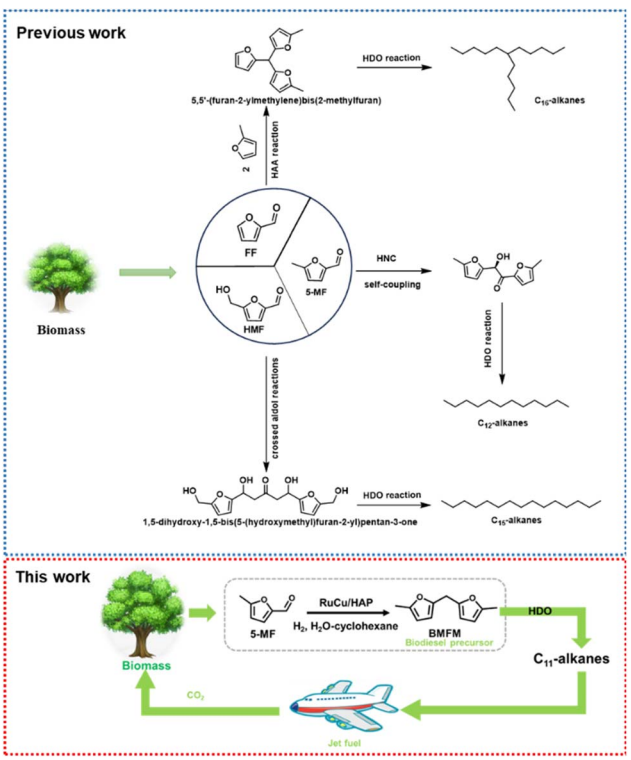

Scheme 1 The typical approaches of jet fuel production from biomass-derived furanic aldehydes.

[a]*Key Laboratory of Poyang Lake Environment and Resource Utilization (Nanchang University) Ministry of Education, School of Resources & Environment, Nanchang University, Nanchang 330031, P.R. China. E-mail: liuzhengli@ncu.edu.cn*

[b]*School of Chemistry and Chemical Engineering, Nanchang University, Nanchang 330031, P.R. China. E-mail: wyang16@ncu.edu.cn*

† Electronic supplementary information (ESI) available. See DOI: https://doi.org/10.1039/d5ra02666k

‡ These authors contributed equally to this work.

platform molecules, including 5-hydroxymethylfurfural (HMF),[4,5] 5-methylfurfural (5-MF),[6–10] and furfural (FF),[11,12] has attracted significant interest.[13] Although direct hydrodeoxygenation of these C_5–C_6 compounds produces corresponding short-chain biofuels,[14–16] strategic carbon chain elongation enables the synthesis of C_9–C_{20} hydrocarbons.[17,18] Subsequent hydrodeoxygenation of these extended structures generates long-chain alkanes suitable for aerospace fuel applications.[19,20]

Currently, various technologies have been developed to extend the carbon chains of furanic aldehydes (Scheme 1), including hydroxyl alkylation/alkylation (HAA) reactions,[21–23] aldol condensation,[24,25] aerobic oxidative condensation,[26] and pinacol C–C coupling[27,28] *etc.* For example, Corma *et al.* used sulfuric acid and *p*-toluenesulfonic acid as catalysts for the reaction of 2-MF with FF to produce trifuran oligomers.[29] Shi *et al.* successfully achieved the selective increase of carbon chain length through the aerobic oxidative condensation of furfural and straight-chain alcohols using a Cu_2O–LiOH catalytic system.[26] Fu's group achieved pinacol C–C coupling of both furfural (FA) and 5-methyl furfural (5-MF) using active metals (Mg, Al, or Zn) in NaOH solution.[27] Abu-Omar *et al.* employed NHC catalysts to achieve nearly 90% yield of self-coupled product from 5-MF.[30] Subsequently, they successfully converted 5,5′-dimethylfuran to *n*-dodecane with 94% selectivity using zeolite-supported Pd catalysts. However, these methods typically require either additional acid/base catalysts or overstoichiometric metal reducing agents. Therefore, developing milder catalytic systems for bio-based furan aldehyde coupling remains highly desirable. 5-MF is an important biomass platform chemical, that is more stable than HMF and can be readily derived from cellulose, fructose and starch.[6–10] In previous work, we found that 5-methylfurfuryl alcohol (5-MFA) can undergo self-condensation to form fuel precursor without catalysts under air atmosphere.[31] Nevertheless, this approach requires $NaBH_4$ for the initial reduction of 5-MF to 5-MFA, presenting a significant limitation.

Herein, we developed a RuCu/HAP catalyst for the direct selective self-condensation of 5-MF to C_{11} products, achieving a 75.6% yield of bis(5-methylfuran)methane (BMFM), Furthermore, a 79% yield of C_{11} straight-chain alkanes was obtained from BMFM through the hydrodeoxygenation (HDO) process. Mechanistic studies elucidated that Ru mediates hydrogenation steps *via* C=O activation, while Cu orchestrates acid sites essential for self-condensation of 5-MFA. The synergistic interplay between metallic Ru and acidic Cu sites thereby enables simultaneous optimization of conversion efficiency and BMFM selectivity. This innovative catalytic strategy provides a sustainable alternative pathway for the synthesis of advanced biofuel precursors.

2 Experimental

2.1 Chemicals

5-Methylfurfural, 5-methylfurfuryl alcohol, 5-methyltetrahydrofurfuryl alcohol, and 2,5-hexanedione were purchased from Shanghai Macklin Biochemical Co., Ltd. $RuCl_3$ (ruthenium(III) chloride) and $Cu(NO_3)_2 \cdot 3H_2O$ (copper nitrate trihydrate) were obtained from Anhui Senrise Technologies Co., Ltd and Shanghai Aladdin Biochemical Technology Co., Ltd, respectively. Cyclohexane, hydroxyapatite (HAP), toluene, ethyl acetate, dichloromethane, and formaldehyde were obtained from Beijing Innochem Science &Technology Co., Ltd.

2.2 Catalyst preparation

Catalysts with varying metal ratios (RuCu/HAP, Cu/HAP, and Ru/HAP) were prepared *via* the impregnation method. Briefly, 0.5 g of hydroxyapatite (HAP) was uniformly dispersed in 15 mL of deionized water under stirring. Separately, 20.5 mg of $RuCl_3$ and 190 mg of $Cu(NO_3)_2 \cdot 3H_2O$ were dissolved in 15 mL of deionized water and stirred for 10 min to ensure homogeneity. The metal salt solution was then slowly added to the HAP suspension. The mixture was stirred at room temperature (RT) for 24 h at 600 rpm, followed by centrifugation and washing three times with deionized water. The obtained solid was dried overnight in a vacuum oven and subsequently reduced under H_2/Ar (10%) flow (100 mL min^{-1}) at 400 °C for 4 h with a heating rate of 10 °C min^{-1}. The final catalysts were denoted as RuCu/HAP (Ru 2 wt%, Cu 10 wt%), Ru/HAP (Ru 2 wt%), and Cu/HAP (Cu 10 wt%), respectively. Detailed preparation methods for Zr/NC, Cu/NC, Ru-MgAl-LDH and Ni-MOF were described in ESI.†

2.3 Catalyst characterizations

X-ray diffraction (XRD) patterns were acquired using a Panalytical Empyrean diffractometer with Cu-Kα radiation. The morphology of the samples was examined by transmission electron microscopy (TEM, JEOL 2100F). Surface chemical composition and elemental oxidation states were analyzed *via* X-ray photoelectron spectroscopy (XPS, Thermo Scientific K-Alpha) equipped with an Al Kα X-ray source. Acid site densities of the catalysts were determined by ammonia temperature-programmed desorption (NH_3-TPD) on an AutoChem II 2950 analyzer. Brunauer–Emmett–Teller (BET) surface areas and pore volumes were measured through nitrogen physisorption at 77 K using a Quantachrome Autosorb iQ instrument (Quantachrome Corp., USA). Prior to BET analysis, samples were degassed at 150 °C for 6 h under vacuum. Inductively coupled plasma optical emission spectrometry (ICP-OES) was conducted on a Thermo Fisher iCAP 7400 to quantify bulk metal concentrations.

2.4 Catalyst performance evaluation and product analysis

All reactions were conducted in a high-pressure stainless-steel reactor (CHEMNNSC50-P5-T3-HC1-SV), temperature controller and IKA magnetic stirring device were purchased from Anhui Chem-n Instrument Co., Ltd. Typically, reactants and solvents were loaded into the reactor, and the reaction was performed at the predetermined temperature under hydrogen atmosphere. After reaction completion, the reaction system was cooled to room temperature. The reaction mixture was collected and filtered through a 0.22 μm syringe filter. The organic phase was analyzed by gas chromatography-mass spectrometry (GC-MS,

Thermo Scientific TRACE 1310) using a chromatographic column (HP-5 capillary column: 30 m × 320 μm × 0.25 μm) and gas chromatography (GC, Agilent 7820A gas) using a chromatographic column (HP-5 capillary column: 30 m × 320 μm × 0.25 μm). The aqueous phase was analyzed by ultra performance liquid chromatography (UPLC, Waters, Acquity H-class) using an organic acid column (Alltech OA1000-organic acid column: 6.5 mm ID × 300 mm). The calibration curve was obtained by preparing the standard solution, and the compound concentration was calculated by external standard method. The conversion rate of 5-MF and yield of BMFM were calculated using the following formula:

$$5-\text{MF conversion} = \frac{\text{Moles of initial 5-MF} - \text{Moles of final 5-MF}}{\text{Moles of initial 5-MF}} \times 100$$

$$\text{BMFM yield} = \frac{2 \times \text{moles of final BMFM}}{\text{moles of initial 5-MF}} \times 100$$

3 Results and discussion

3.1 Catalytic process development

Table 1 summarizes the catalytic performance of various catalysts in the self-condensation of 5-methylfurfural (5-MF). Notably, Zr/NC and Cu/NC exhibited negligible catalytic activity with undetectable BMFM formation (Table 1, entries 1–2). Although Ru-MgAl-LDH and Ni-MOF achieved 69% substrate conversion, they demonstrated limited product selectivity with merely 2% and 3.2% BMFM yields, respectively (Table 1, entries 3–4). This phenomenon could be attributed to the distinct catalytic functionalities: Ru sites exhibit superior C=O bond hydrogenation capacity, whereas Cu incorporation modulates the acid sites equilibrium. This synergistic interplay underpins the enhanced activity of bimetallic RuCu catalysts relative to their monometallic analogues.[32] The synthesized RuCu/HAP catalyst delivered an initial BMFM yield of 36.0% (Table 1, entry 5). Through systematic optimization of reaction parameters (cyclohexane/water volume ratio 1 : 1, H_2 pressure 4 MPa, 100 °C, 4 h), the BMFM yield was remarkably enhanced to 75.6%, representing 2.6-fold and complete improvements over Ru/HAP (28.7%) and Cu/HAP (no detectable product), respectively (Table 1, entries 6–9). Compared with commercial Ru/C, RuCu/HAP also showed higher yield for (BMFM) (Table 1, entry 10). Scalability assessment under gram-scale conditions confirmed practical applicability (Table 1, entry 11), with product verification through GC-MS and NMR analyses (Fig. S1–S3†).

Table 1 Exploration and optimization of the reaction conditions[a]

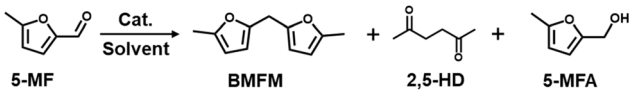

Entry	Catalyst	Conversion (%)	Yield (%)		
			BMFM	2,5-HD	5-MFA
1	Zr/NC	27.8	0	0	16.2
2	Cu/NC	15.3	0	0	3.2
3	Ru–MgAl-LDH	69.0	2	0	4.4
4	Ni-MOF	32.2	3.2	0	15.2
5	RuCu/HAP	100	36.0	37.8	0
6	HAP[b]	0	0	0	0
7	Cu/HAP[b]	18.3	0	2.5	0
8	Ru/HAP[b]	64.8	28.7	10.2	4.8
9	RuCu/HAP[b]	100	75.6	13.0	0
10	Ru/C[b]	100	35.0	20.6	0
11	RuCu/HAP[c]	100	63.9	18.4	6.9

[a] Reaction conditions: 5-MF (1 mmol), catalyst (50 mg), cyclohexane (5 mL) and water (5 mL),140 °C, H_2 (4 MPa), 4 h. [b] 5-MF (1 mmol), catalyst (50 mg), cyclohexane (5 mL) and water (5 mL),100 °C, H_2 (4 MPa), 4 h. [c] 5-MF (1.1 g, 10 mmol), catalyst (100 mg), cyclohexane (10 mL) and water (10 mL), 100 °C, H_2 (4 MPa),12 h. Note: H_2 will be consumed quickly, additional H_2 should be added to maintain H_2 pressure >4 MPa during the reaction process.

Furthermore, the BMFM underwent sequential hydrodeoxygenation (HDO) catalyzed by a Pd/C and H-Beta zeolite system, resulting in its conversion to C_{11} straight-chain alkanes. This catalytic process achieved a C_{11} biofuel yield of 79% (Fig. S4 and S5†). In contrast to conventional lipid-derived biodiesels (C_{17}–C_{18} hydrocarbons with freezing points ranging from 22 to 29 °C),[33] the synthesized C_{11} straight-chain alkanes exhibits characteristics of light diesel oil with a significantly lower freezing point of −26 °C. This enhanced low-temperature fluidity suggests promising potential for cold-climate applications.

Hydrocarbons hydrodeoxygenation (HDO) optimization: BMFM (2 mmol, 352 mg), Pd/C (5.0 wt%, 50 mg), H-beta zeolite (50 mg) and 10 mL cyclohexane were added to a 25 mL high pressure reactor. The reactor was purged three times with nitrogen and then charged with 4 MPa H_2. Then the reactor was heated to 190 °C under vigorous stirring for 10 h. After the system cooled down to room temperature, the catalyst was removed by filter and analyzed by GC-MS and GC, 79% yield C_{11} straight-chain alkanes was obtained (GC).

A systematic investigation of reaction parameters revealed critical structure–activity relationships. Temperature dependence studies (Fig. 1a) demonstrated marked thermal effects: At 80 °C, 5-methylfurfuryl alcohol (5-MFA) predominated with 93.7% yield, whereas BMFM production remained marginal (4.6%). Remarkably, elevating the temperature to 100 °C induced complete consumption of 5-MFA concomitant with a substantial increase in BMFM yield to 75.6%, alongside 13% yield of ring-opening product 2,5-hexanedione (2,5-HD). Hydrogen pressure optimization at 100 °C established 4 MPa H_2 as the optimal condition for BMFM production (75.6% yield, Fig. 1b). Beyond this threshold, over-hydrogenation phenomena became increasingly pronounced, adversely affecting product selectivity.

The solvent system exerted a significant influence on the reaction outcomes (Fig. 1c and d). In the water-dichloromethane (DCM) biphasic system, a low substrate

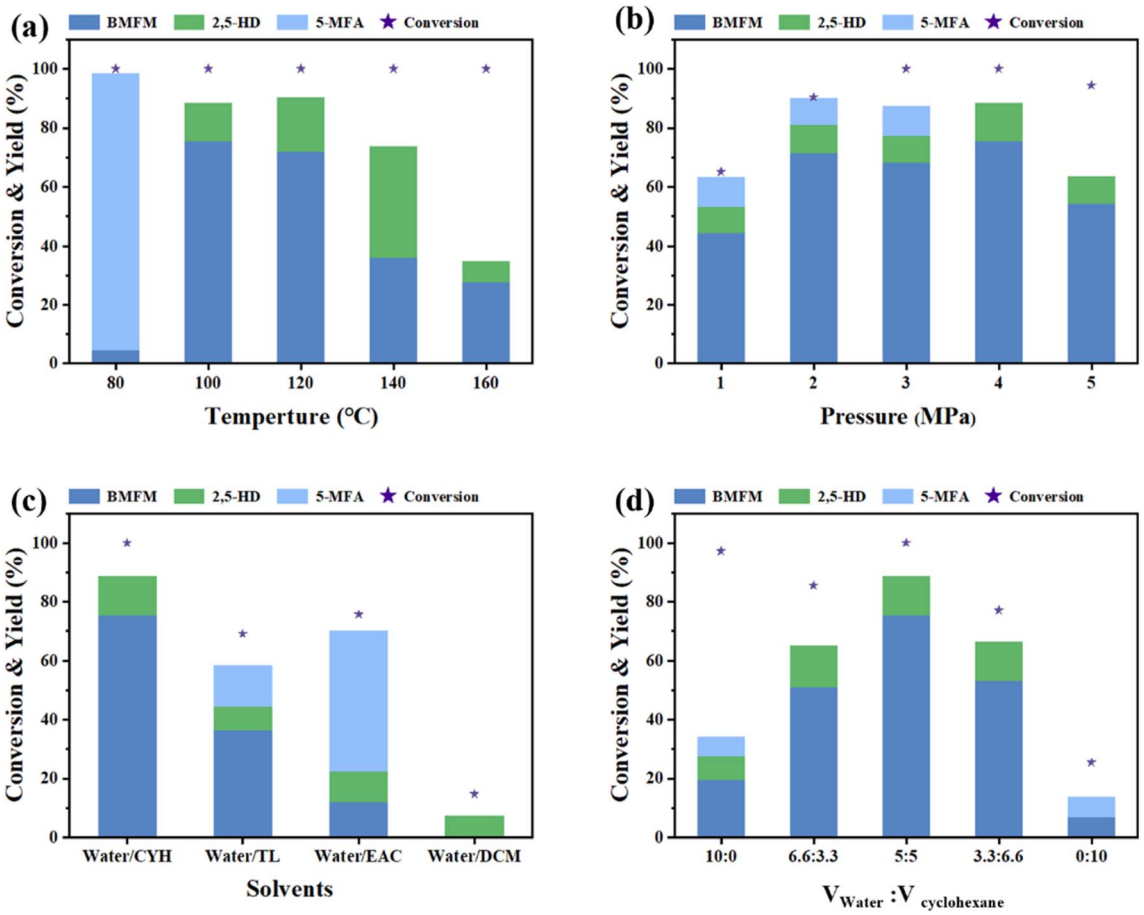

Fig. 1 Effect of (a) reaction temperatures, (b) hydrogen pressures (reaction conditions: 1 mmol 5-MF, 50 mg RuCu/HAP, $V_{cyclohexane} : V_{water} = 1 : 1$), H_2 (4 MPa), 4 h. Effect of (c) organic solvents types and (d) the volume proportion of cyclohexane.

conversion of 14.8% was observed, yielding 7.3% 2,5-hexanedione (2,5-HD) without detectable formation of the target product (BMFM). By contrast, the water-ethyl acetate (EA) system demonstrated markedly enhanced catalytic performance, achieving 75.7% 5-MF conversion with 47.6% yield of 5-MFA as the primary product, accompanied by minor quantities of 2,5-HD (10.6%) and BMFM (12%). The water-toluene system achieved 69.1% substrate conversion and generated BMFM in 36.6% yield. Notably, the water-cyclohexane biphasic system exhibited complete substrate conversion (100%) and delivered the highest BMFM yield of 75.6%.

Further investigation revealed that water/cyclohexane volume ratios (6.6 : 3.3 and 3.3 : 6.6 v/v) led to incomplete conversions, whereas the 5 : 5 v/v ratio achieved optimal efficiency. In monophasic systems, aqueous conditions afforded 97.2% substrate conversion but only 19.7% selectivity toward BMFM, indicating that water-mediated activation promotes conversion but simultaneously induces competing side reactions. Conversely, pure cyclohexane exhibited limited catalytic activity, with both low conversion (12.4%) and BMFM selectivity (8.9%). These results suggest a synergistic mechanism in the biphasic system: The aqueous phase facilitates substrate activation through polar interactions, while the organic phase minimizes side reactions through solvation effects and continuous product extraction. This phase-separation strategy successfully reconciles the conflicting requirements for high substrate conversion and product selectivity that single-phase systems cannot simultaneously satisfy.

The effect of the Ru and Cu loading ratio on the reaction was systematically investigated, as presented in Table S1.† Initially, a catalyst containing 2% ruthenium metal was employed to catalyze the reaction (Table S1,† entry 1), resulting in a substrate conversion rate of 64.8% and a BMFM yield of 28.7%. Upon incorporating copper (Table S1,† entries 2–4), the substrate conversion rate with 5% Cu loading was slightly higher than that without Cu doping, while the selectivity for BMFM significantly improved. Increasing the Cu loading to 10% led to a BMFM yield of 75.6%. However, further increasing the Cu content to 15% caused a decrease in the conversion rate of 5-MF, potentially due to reduced reaction activity caused by excessive Cu coating on the ruthenium metal. When the catalyst was loaded with 10% Cu (Table S1,† entry 5), the conversion rate of 5-methylfurfural reached 18.3%, but no BMFM was detected. Subsequently, the ruthenium content was adjusted from 0% to 3%, revealing that the highest BMFM yield was achieved at 2% ruthenium loading (Table S1,† entries 5–7). Further increasing

the ruthenium content resulted in a decreased BMFM yield. Consequently, the optimized metal ratio determined is a Ru : Cu ratio of 2 : 10.

To evaluate catalyst stability, the RuCu/HAP catalyst was recovered after each reaction cycle *via* centrifugation, washed thoroughly, and dried under vacuum at 60 °C for subsequent reuse. As shown in Fig. S6,† the catalyst maintained stable activity over the first four cycles, with consistent 5-MF conversion and BMFM yield (~75.6%). However, by the fifth cycle, the conversion decreased to 81.6%, accompanied by a decline in BMFM yield to 55%. ICP-OES analysis revealed metal leaching during recycling, with Cu content decreasing from 10.47 wt% to 7.7 wt% and Ru content from 1.58 wt% to 1.22 wt% (Table S2†). Furthermore, TEM and SEM characterization confirmed that the metal nanoparticles retained their original size (~2.38 nm) and morphology without significant agglomeration, indicating good structural stability (Fig. S7†). Additionally, SEM observations indicated that both Ru and Cu were still dispersed well within the catalyst structure. The content of weakly acidic sites was significantly decreased, which indicates that a moderate amount of acidity is crucial for maintaining high BMFM selectivity (Table S3†).

3.2 Catalyst characterization

Based on the above results of catalytic performance tests, the structure and catalytic activity relationship of catalysts were explored. The structures of catalysts were further characterized. The crystal structures of the catalysts were characterized by X-ray Diffraction (XRD). The XRD patterns of carrier HAP, HAP loaded with single metal Ru (2 wt%) or Cu (10 wt%), and bimetals (2 wt% Ru, 10 wt% Cu) were shown in Fig. 2. Distinct characteristic peaks at 25.8°, 31.8°, 32.9°, 34.1°, 46.7° and 49.4° could be observed, which correspond to the diffraction peaks of HAP,[34] indicating the stability of hydroxyapatite after loading and calcination processes. No discernible characteristic peaks related to Ru species were detected in Ru/HAP samples, possibly due to its good dispersity and low loading amount on the HAP surface. The characteristic peaks at 43.2°, 50.4° and 74.1° in Cu/HAP could be attributed to the crystal faces of Cu^0 (111), (200) and (220).[35] In contrast, no distinct characteristic peaks associated with Ru species were found in RuCu/HAP samples, suggesting a highly dispersed state for the incorporated Ru metal within the catalyst structure. A significant reduction in intensity was observed for the Cu^0 diffraction peak of RuCu/HAP compared to that of pure Cu/HAP sample due to enhanced dispersion resulting from the Ru addition.

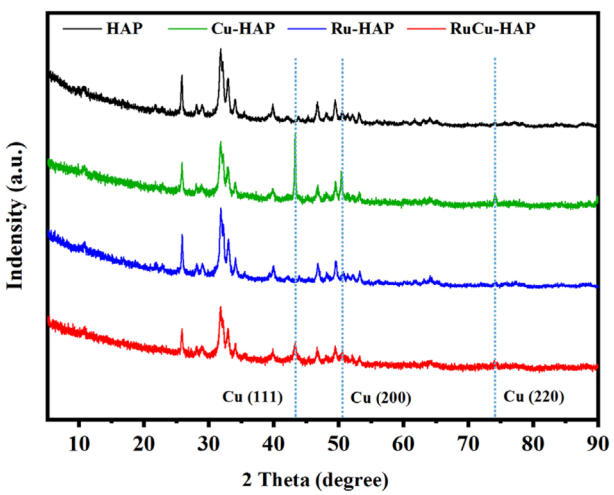

Fig. 2 Powder XRD patterns of catalysts.

Table 2 The N_2 adsorption–desorption data of HAP, Cu/HAP, Ru/HAP and RuCu/HAP catalysts

Entry	Catalyst	S_{BET} ($m^2\ g^{-1}$)	V_{total} ($cm^3\ g^{-1}$)	$d_{avg.}$ (nm)
1	HAP	65.203	0.269	16.541
2	Cu/HAP	40.286	0.211	21.036
3	Ru/HAP	59.428	0.293	19.727
4	RuCu/HAP	47.113	0.254	21.627

The N_2 adsorption–desorption method was employed to assess the structural properties of the catalysts, and the results were presented in Table 2 and Fig. S8.† The HAP vector exhibited a type III isotherm, indicating a macroporous structure. The Brunauer-Emmet-Teller (BET) specific surface area of HAP was determined to be 65.203 $m^2\ g^{-1}$, while the specific surface area of Cu/HAP decreased to 40.286 $m^2\ g^{-1}$, potentially due to the loading of Cu nanoparticles. In contrast, there was only a slight decrease in the specific surface area of Ru/HAP (59.428 $m^2\ g^{-1}$) due to good dispersity and low metal loading of Ru, which is consistent with the XRD analysis. RuCu/HAP also exhibited decreased surface area (47.113 $m^2\ g^{-1}$), but remained higher than that of Cu/HAP possibly due to better Cu dispersion by Ru metal addition.

Transmission electron microscope (TEM) was performed to characterize the surface morphology and microstructure of the catalysts. As presented in Fig. 3a, HAP predominantly exhibited an elongated bar shape, while the loaded Ru and Cu particles appeared spherical, ranging in size from 1.0 to 3.5 nm with an average particle size of 2.3 nm. Additionally, the TEM and SEM analyses of Cu/HAP revealed that the particle size distribution in Cu/HAP ranges from 2.0 nm to 7.0 nm, with an average particle size of 4.3 nm, approximately twice as large as those observed in RuCu/HAP (Fig. 3b). Notably, the particle size of Ru/HAP (Fig. 3c) was slightly smaller than that of RuCu/HAP (the particle size distribution for Ru/HAP falls between 0.5 and 2.5 nm, with an average particle size of 1.46 nm), indicating that the incorporation of Ru hinders the growth of Cu particles, which is also consistent with previous XRD analysis results. Furthermore, SEM imaging coupled with elemental maps (Fig. 3d–i) demonstrated uniform dispersion of both Ru particles and Cu particles within HAP.

The surface chemical states of the prepared catalysts were characterized by X-ray photoelectron spectroscopy, as shown in Fig. 4. For the high-resolution Cu 2p spectra, in the case of RuCu/HAP, the peaks at 932.6 eV and 934.3 eV corresponded to the characteristic peaks of Cu^0 and Cu^{2+} in $2p_{3/2}$ orbits. The peaks at 952.2 eV and 954.2 eV were the characteristic peaks of

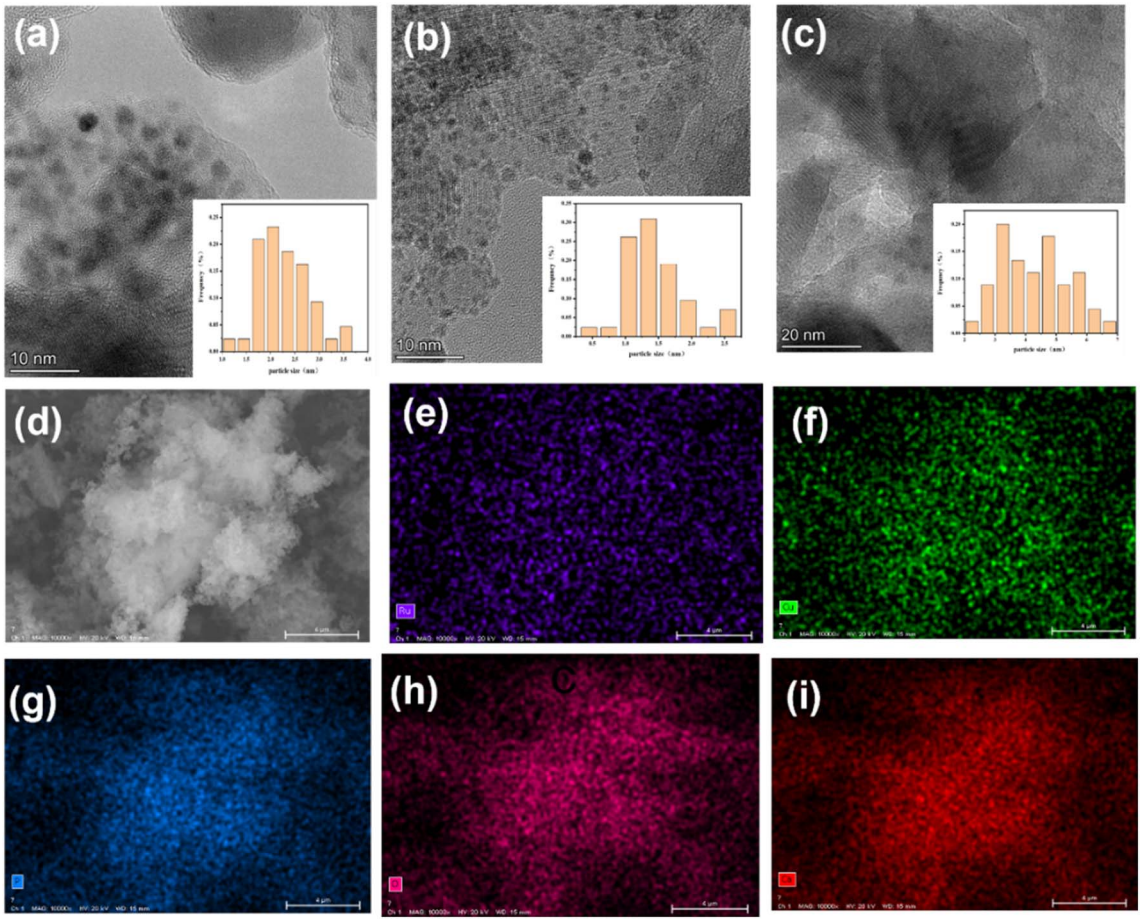

Fig. 3 High-resolution transmission electron micrographs (HR-TEM), and particle size distributions of (a) RuCu/HAP, (b) Ru/HAP and (c) Cu/HAP. (d–i) scanning electron micrograph (SEM) and corresponding elemental mappings of RuCu/HAP.

Cu^0 and Cu^{2+} in $2p_{1/2}$ orbits. The presence of Cu^{2+} was attributed to incomplete reduction of some Cu species. The peaks at 462.2 eV and 484.5 eV were assigned as characteristic peaks of Ru in $3p_{3/2}$ and $3p_{1/2}$ orbitals, respectively.

3.3 Mechanistic study

To elucidate the reaction mechanism, time-dependent monitoring was performed under standard catalytic conditions. As depicted in Fig. 5a, the substrate conversion exhibits a progressive increase with reaction duration, achieving complete conversion (100%) within 4 h. The BMFM yield correspondingly reaches 75.6% at the reaction endpoint. While 2,5-HD content increased linearly to 13% by 4 h, the 5-MFA concentration exhibited a monotonic decrease to undetectable levels. In addition, extremely trace amounts of 5,5'-(oxybis(methylene))bis(2-methylfuran) (OBMB) and methanol (MeOH) were also detected in this process (Fig. S9 and S10†). These results indicated that 5-MFA could be a reactive intermediate, whereas 2,5-HD and OBMB may be a terminal byproduct. The methanol may be derived from subsequent hydrogenation of formaldehyde generated during the condensation process of 5-MFA.

To further explore the structure–activity relationship between the catalyst and the reaction, comparative analysis of the catalytic performance among Cu/HAP, Ru/HAP, and RuCu/HAP toward 5-MF and 5-MFA was conducted. As depicted in Fig. 5b, Cu/HAP exhibited low catalytic activity when 5-MF was used as the substrate, achieving a BMFM yield of only 70.5% with 5-MFA. This suggests that Cu possesses weak hydrogenation activity toward C=O bonds and predominantly facilitates the self-condensation of 5-MFA into BMFM. Notably, Ru/HAP demonstrated a BMFM yield of 28.7% with 5-MF, attributable to its enhanced C=O hydrogenation capability compared to Cu. Conversely, no BMFM formation (0% yield) was observed for Ru/HAP using 5-MFA, with 5-MTHFA emerging as the primary product (yield: 86.2%). Remarkably, RuCu/HAP achieved superior BMFM yields of 75.6% and 88.8% using 5-MF and 5-MFA as substrates, respectively. The distinct catalytic performances between RuCu/HAP and Ru/HAP likely stem from Cu-induced modifications in substrate adsorption configurations on Ru/HAP surfaces.

To validate above hypothesis, attenuated total reflectance infrared (ATR-IR) spectroscopic was employed to investigate the adsorption configurations of 5-MF on different catalytic surfaces (Fig. 5c). For Ru/HAP catalysts, characteristic peak

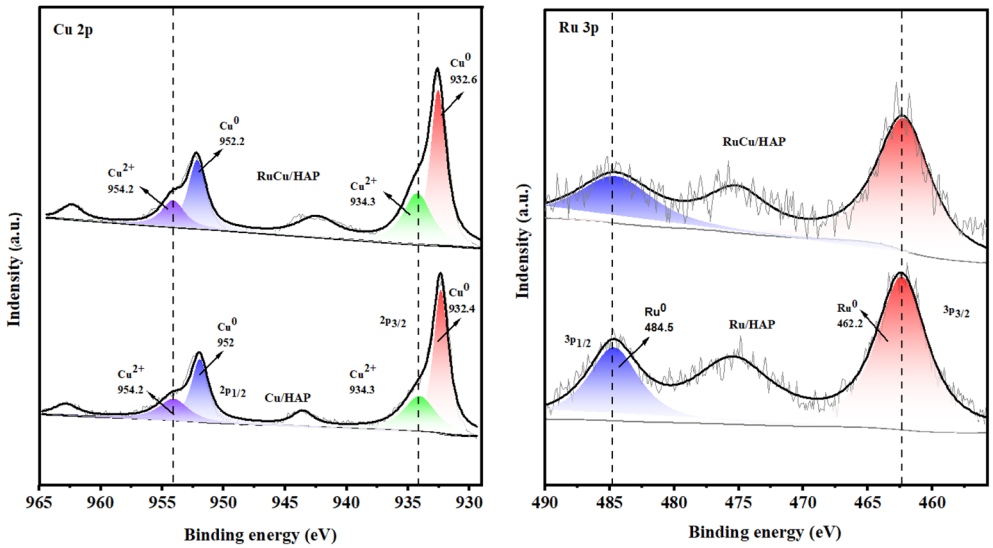

Fig. 4 High-resolution XPS of the monometallic and bimetallic catalysts for (a) Cu $2p_{3/2}$, (b) Ru $3p_{3/2}$.

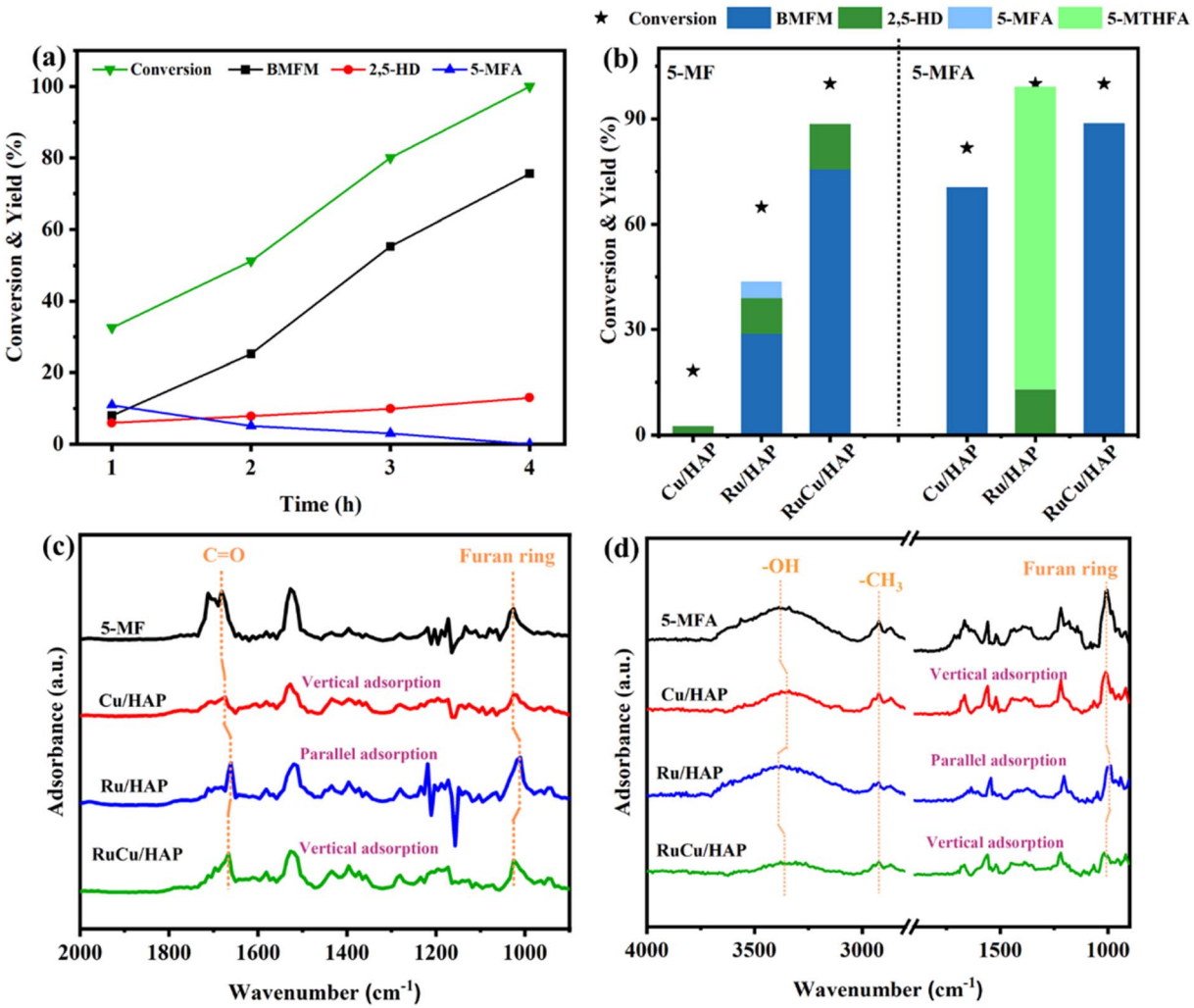

Fig. 5 (a) 5-MF conversion and products yield at different reaction times, reaction conditions: 5-MF (1 mmol), catalyst (50 mg), cyclohexane (5 mL) and water (5 mL), 100 °C, H_2 (4 MPa), 4 h. (b) Conversion of 5-MFA with different catalysts. (c) ATR-IR spectra of 5-MF adsorbed over catalysts; (d) ATR-IR spectra of 5-MFA adsorbed over catalysts.

Table 3 Acid site number of HAP, Cu/HAP, Ru/HAP, RuCu/HAP

Catalyst	Weak acidity (mmol g^{-1})	Medium acidity (mmol g^{-1})	Strong acidity (mmol g^{-1})	Total acidity (mmol g^{-1})
HAP	0.176	0.297	0	0.473
Cu/HAP	0.147	0	0.789	0.936
Ru/HAP	0.378	0.094	0.095	0.567
RuCu/HAP	0.369	0.101	0.421	0.931

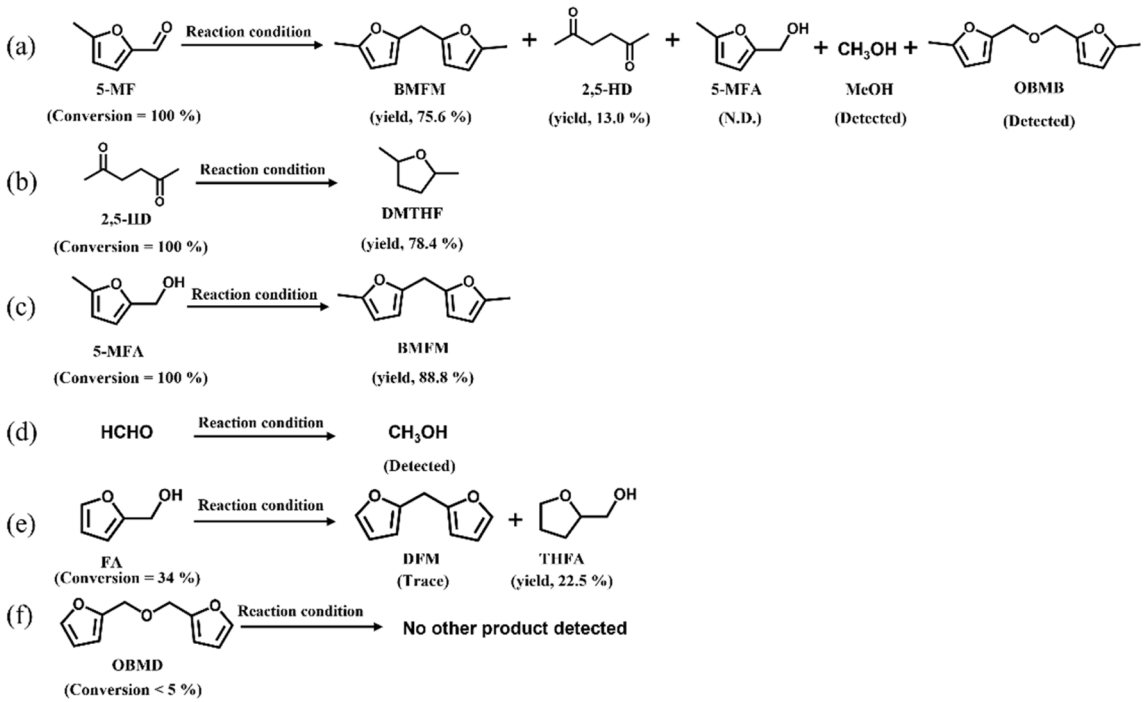

Scheme 2 Control experiments. Reaction conditions: substrate (1 mmol), RuCu/HAP (50 mg), cyclohexane (5 mL) and water (5 mL), 100 °C, H_2 (4 MPa), 4 h.

shifts were observed in both the furan ring (1025 → 1010 cm^{-1}) and carbonyl (C=O) group (1681 → 1661 cm^{-1}), suggesting a planar adsorption configuration.[36] In contrast, RuCu/HAP and Cu/HAP systems exhibited selective modification of the C=O vibration (redshifted to 1671 cm^{-1}) while maintaining the original furan ring signature at 1025 cm^{-1}. Regarding 5-MFA adsorption (Fig. 5d), vertical configurations were observed on Cu/HAP and RuCu/HAP surfaces, whereas a parallel adsorption configuration dominated on Ru/HAP. This result further demonstrates that the distinct catalytic performance between RuCu/HAP and Ru/HAP likely originates from Cu-induced alterations in substrate adsorption geometry on the Ru/HAP surface.

In addition, the acidic sites on the surface of the catalyst may also have a significant impact on the synthesis of BMFM. Thus, NH_3-TPD analysis was systematically performed (Fig. S11†). Quantitative assessment unveiled comparable acid site densities for Cu/HAP (0.936 mmol g^{-1}) and RuCu/HAP (0.931 mmol g^{-1}), both significantly exceeding those of Ru/HAP (0.567 mmol g^{-1}) and pristine HAP (0.473 mmol g^{-1}) (Table 3).

To sum up, Ru mediates hydrogenation steps *via* C=O activation, while Cu orchestrates acid sites essential for self-condensation of 5-MFA. The synergistic interplay between metallic Ru and acidic Cu sites thereby enables simultaneous optimization of conversion efficiency and BMFM selectivity.

To further clarify the catalytic reaction path, control experiments were further conducted (Scheme 1). The experimental results (a–f) demonstrated that under same reaction conditions, the BMFM yield reached 88.8% when using 5-MFA as the substrate. In contrast, 2,5-dimethyltetrahydrofuran (DMTHF) emerged as the primary product when 2,5-HD served as the substrate, confirming that 5-MFA functions as the reaction intermediate while 2,5-HD represents a by-product. The experimental (d) result revealed that methanol can be originated from the hydrogenation of formaldehyde. Since OBMB is difficult to obtain, investigations were conducted using its structural analog OBMD. Results from experiments (e) and (f) indicated trace amounts of di(furan-2-yl)methane (DFM) detection when employing furfuryl alcohol as the substrate (Fig. S12†), whereas no DFM was detected when OBMD was

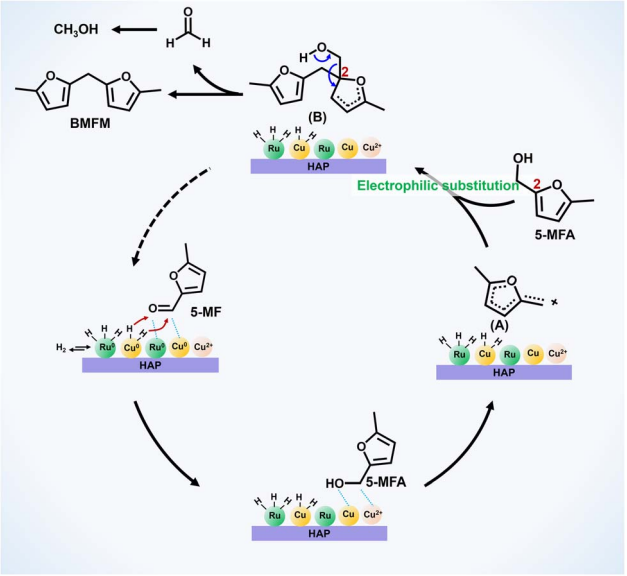

Scheme 3 A possible reaction mechanism for the direct conversion of 5-MF to BMFM over the Ru Cu/HAP catalyst.

utilized. Collectively, these findings establish 5-MFA as the key reaction intermediate, with 2,5-HD and OBMB identified as process by-products. The methanol formation likely derives from subsequent hydrogenation of formaldehyde generated during the condensation process of 5-MFA (Fig. S13† and Scheme 2).

According to the aforementioned results and related literature,[37–41] As illustrated in Scheme 3, a possible reaction mechanism was proposed. Initially, 5-MF underwent hydrogenation to form 5-MFA over the RuCu/HAP catalyst. Subsequently, the 5-MFA molecule was dehydrated at the Lewis acid sites present on the RuCu/HAP surface, generating a delocalized carbocation intermediate (A). This carbocation intermediate then participated in an electrophilic substitution reaction with the C2 position of the furan ring in another 5-MFA molecule, yielding an unstable dimeric intermediate (B). The intermediate B underwent intramolecular electron transfer to produce BMFM, concomitantly releasing a formaldehyde molecule. The liberated formaldehyde was subsequently hydrogenated to methanol.

4 Conclusion

In summary, this work successfully addresses the challenge of selective synthesis of bis(5-methylfuran)methane (BMFM) from biomass-derived 5-methylfurfural (5-MF) by designing a synergistic bimetallic RuCu/hydroxyapatite (HAP) catalyst. The RuCu/HAP system achieves an exceptional BMFM yield of 75.6% under mild conditions, outperforming monometallic Ru or Cu catalysts by effectively suppressing undesired side reactions. Mechanistic studies reveal that the catalytic synergy stems from the distinct roles of Ru and Cu: Ru facilitates hydrogenation *via* C=O activation, while Cu-derived acid sites promote the self-condensation of intermediates. Furthermore, the downstream hydrodeoxygenation (HDO) of BMFM delivers a 79% yield of C11 straight-chain alkanes, demonstrating the viability of this pathway for producing renewable drop-in biofuels. This study not only advances the catalytic valorization of lignocellulosic biomass but also presents a rational design strategy for bifunctional catalysts, balancing hydrogenation and acid-catalyzed steps. The results hold significant promise for sustainable aviation fuel production, bridging the gap between renewable feedstocks and high-performance energy carriers. Future efforts should focus on optimizing catalyst stability and scaling the process to accelerate industrial adoption.

Data availability

The data supporting this study have been included as part of the ESI.†

Author contributions

Conghao Ku: writing–original draft, visualization, methodology, investigation, formal analysis, data curation, conceptualization. Jiaming Tang: data curation, conceptualization, methodology, investigation, writing–original draft. Xucheng Li: investigation, data curation. Zhengli Liu: writing – review & editing, supervision, project administration. Weiran Yang: writing – review & editing, supervision, project administration, funding acquisition.

Conflicts of interest

There are no conflicts to declare.

Acknowledgements

This work was supported by the National Natural Science Foundation of China (No. 22169011).

References

1 L. T. Mika, E. Cséfalvay and Á. Németh, *Chem. Rev.*, 2018, **118**, 505–613.
2 R. Lødeng, C. Ranga, T. Rajkhowa, V. I. Alexiadis, H. Bjørkan, S. Chytil, I. H. Svenum, J. Walmsley and J. W. Thybaut, *Biomass Convers. Biorefin.*, 2017, **7**, 343–359.
3 Q. Liu, X. Zhang, Q. Zhang, Q. Liu, C. Wang and L. Ma, *Energy Fuels*, 2020, **34**, 7149–7159.
4 G. Yong, Y. Zhang and J. Y. Ying, *Angew. Chem., Int. Ed.*, 2008, **47**, 9345–9348.
5 J. B. Binder and R. T. Raines, *J. Am. Chem. Soc.*, 2009, **131**, 1979–1985.
6 W. Guan, Y. Zhang, C. Yan, Y. Chen, Y. Wei, Y. Cao, F. Wang and P. Huo, *ChemSusChem*, 2022, **15**, e202201041.
7 R. Xie, W. He, G. Qu, H. Wu, Z. Li, J. Li and W. Li, *BioEnergy Res.*, 2023, **16**, 1108–1120.
8 Y. Peng, X. Li, T. Gao, T. Li and W. Yang, *Green Chem.*, 2019, **21**, 4169–4177.

9 J. Xu, X. Miao, L. Liu, Y. Wang and W. Yang, *ChemSusChem*, 2021, **14**, 5311–5319.
10 M. R. Grochowski, W. Yang and A. Sen, *Chem. - Eur. J.*, 2012, **18**, 12363–12371.
11 Q. Xia, H. Peng, Y. Zhang, G. Fu, Y. Liu, Z. Xiao, L. Huang and H. Bi, *Biomass Convers. Biorefin.*, 2021, **13**, 7895–7907.
12 E. I. Gürbüz, J. M. R. Gallo, D. M. Alonso, S. G. Wettstein, W. Y. Lim and J. A. Dumesic, *Angew. Chem., Int. Ed.*, 2013, **52**, 1270–1274.
13 F. Chen, N. Li, S. Li, G. Li, A. Wang, Y. Cong, X. Wang and T. Zhang, *Green Chem.*, 2016, **18**, 5751–5755.
14 W. Guo, H. Liu, S. Zhang, H. Han, H. Liu, T. Jiang, B. Han and T. Wu, *Green Chem.*, 2016, **18**, 6222–6228.
15 L. Grazia, D. Bonincontro, A. Lolli, T. Tabanelli, C. Lucarelli, S. Albonetti and F. Cavani, *Green Chem.*, 2017, **19**, 4412–4422.
16 T. Thananatthanachon and T. B. Rauchfuss, *Angew. Chem., Int. Ed.*, 2010, **49**, 6616–6618.
17 A. Corma, O. d. l. Torre and M. Renz, *Energy Environ. Sci.*, 2012, **5**, 6328–6344.
18 Y. Nakagawa, M. Tamura and K. Tomishige, *Fuel Process. Technol.*, 2019, **193**, 404–422.
19 S. Sun, R. Yang, X. Wang and S. Yan, *Data Brief*, 2018, **17**, 638–646.
20 X. Li, X. Zeng and Y. Zhang, *Fuel Process. Technol.*, 2022, **232**, 107263.
21 E. C. Atayde, B. M. Matsagar, Y.-C. Wang and K. C. W. Wu, *Appl. Catal., A*, 2024, **669**, 119492.
22 M. R. Singh, C. Xiang and N. S. Lewis, *Sustainable Energy Fuels*, 2017, **1**, 458–466.
23 Q. Xia, Y. Xia, J. Xi, X. Liu, Y. Zhang, Y. Guo and Y. Wang, *ChemSusChem*, 2017, **10**, 747–753.
24 X. Zhao, S. Li, Y. Hu, X. Zhang, L. Chen, C. Wang, L. Ma and Q. Zhang, *Chem. Eng. J.*, 2022, **428**, 131368.
25 S. Shao, W. Dong, X. Li, H. Zhang, R. Xiao and Y. Cai, *J. Cleaner Prod.*, 2020, **250**, 119459.
26 J. Shi, X. Tong, S. Wang and S. Xue, *ACS Catal.*, 2022, **12**, 6029–6035.
27 Y.-B. Huang, Z. Yang, J.-J. Dai, Q.-X. Guo and Y. Fu, *RSC Adv.*, 2012, **2**, 11211–11214.
28 G. Han, X. Liu, Z. Cao and Y. Sun, *ACS Catal.*, 2020, **10**, 9346–9355.
29 A. Corma, O. de la Torre and M. Renz, *ChemSusChem*, 2011, **4**, 1574–1577.
30 B. L. Wegenhart, L. Yang, S. C. Kwan, R. Harris, H. I. Kenttämaa and M. M. Abu-Omar, *ChemSusChem*, 2014, **7**, 2742–2747.
31 S. Qin, T. Li, M. Zhang, H. Liu, X. Yang, N. Rong, J. Jiang, Y. Wang, H. Zhang and W. Yang, *Green Chem.*, 2019, **21**, 6326–6334.
32 Y. Xiao, Y. Wang, J. Zhang, G. Cheng, D. Liang, R. Shan, H. Yuan and Y. Chen, *J. Environ. Chem. Eng.*, 2025, **13**, 115708.
33 S. Qin, T. Li, M. Zhang, H. Liu, X. Yang, N. Rong, J. Jiang, Y. Wang, H. Zhang and W. Yang, *Green Chem.*, 2019, **21**, 6326–6334.
34 J. Dobosz, M. Małecka and M. Zawadzki, *J. Energy Inst.*, 2018, **91**, 411–423.
35 M. V. Morales, E. Asedegbega-Nieto, B. Bachiller-Baeza and A. Guerrero-Ruiz, *Carbon*, 2016, **102**, 426–436.
36 L. Zhang, X. Li, J. Wang, Z. Zeng, W. Yang, S. Deng and Q. Deng, *AIChE J.*, 2023, **69**, e17996.
37 A. T. Balaban, A. Bota and A. Zlota, *Synthesis*, 1980, 136–138.
38 J. A. Marshall and X. J. Wang, *J. Org. Chem.*, 1991, **56**, 960–969.
39 R. I. Khusnutdinov, A. R. Baiguzina, A. A. Smirnov, R. R. Mukminov and U. M. Dzhemilev, *Russ. J. Appl. Chem.*, 2007, **80**, 1687–1690.
40 T. Kim, R. S. Assary, R. E. Pauls, C. L. Marshall, L. A. Curtiss and P. C. Stair, *Catal. Commun.*, 2014, **46**, 66–70.
41 O. S. Attaryan, A. A. Gevorkyan, S. K. Antanosyan and S. G. Matsoyan, *Russ. J. Gen. Chem.*, 2007, **77**, 1139–1140.